Article Identifier
DOI: 10.22032/dbt.58679
URN: urn:nbn:de:gbv:ilm1-2023isc-106:0

60th ILMENAU SCIENTIFIC COLLOQUIUM
Technische Universität Ilmenau, 4 – 8 September 2023
URN: urn:nbn:de:gbv:ilm1-2023isc:1

Development of a Compact DFB Laser Interferometer for High-speed Inline Displacement Measurement

Chen-Yu Liao, Hsi-Hui Lin, Liang-Chia Chen

Precision Metrology Laboratory, Dept. of Mech. Engineering, National Taiwan University, Roosevelt Road Sec. 4, No.1, Taipei 10617, Taiwan

ABSTRACT

A compact fiber laser interferometer, capable of precise displacement measurements, was devised using a 1550 nm DFB laser for frequency modulation up to 300 kHz. The system comprises a fiber laser, a fiber-optic interferometer, and a wavelength modulation system. The presented method offers nanometer-scale precision and incorporates a hydrogen cyanide (HCN) gas cell for monitoring the laser's central wavelength. A technique to compensate for modulation depth has been developed to maintain a consistent modulation depth over extensive measurement ranges. Preliminary trials reveal a measurement bias of less than 40 nm achieved over a 300 mm range at a speed of 100 mm/s compared to a calibrated interferometer. This approach proves beneficial for high-precision measurements for inline semiconductor manufacturing processes.

Index Terms - Nanoscale positioning, Fiber interferometer, HCN gas cell, Wavelength modulation

1. INTRODUCTION

Displacement Measurement Interferometers (DMIs) are vital in various applications necessitating exact positioning capabilities, such as steppers or scanners in semiconductor processing, ultra-precision machining devices, atomic force microscopes, scanning electron microscopes, and nanoscale three-dimensional coordinate measuring machines. Conventional commercial interferometers, large in sensor size and demanding specific optics for measurement [1], are less suited for micron object measurement or integration into machinery for inline process positioning control. Hence, numerous studies have suggested using fiber optics for light and interference signal transmission, facilitating the miniaturization of the interferometer system [2-6]. Fiber optics allows design flexibility in the interferometer and offers the benefit of electromagnetic interference resistance.

Since DMIs employ the wavelength of laser light as a reference for measurement, the light source's wavelength is a crucial factor in DMIs. Numerous studies have addressed laser frequency stabilization, incorporating methods such as using iodine gas absorption lines for helium-neon lasers [7] and the Zeeman stabilization technique [8]. These methods commonly stabilize the laser wavelength by dynamically adjusting the length of the laser cavity, unavoidably leading to a more substantial and complicated sensor structure.

The modulation and demodulation techniques of the interference signal greatly influence the performance of displacement measurement interferometers. The most prevalent

demodulation technique is the Phase-Generated Carrier (PGC) method, introduced by Anthony et al. in 1982 [10]. This method amplifies the interference signal's sensitivity and ensures uniform sensitivity across various phases while mitigating errors caused by light source intensity drift. Multiple strategies exist for modulating the optical phase, including the use of piezoelectric materials to alter the optical path difference [11, 12], the application of an electro-optic modulator (EOM) to generate distinct delays in the optical phase [13], and the modulation of the laser diode's injection current to generate changes in the laser wavelength [14]. Among these techniques, current-wavelength modulation offers high-speed modulation, eliminates the need for additional optical components, and is independent of the polarization state. However, it also has a downside: the modulation depth may fluctuate with the optical path difference, which restricts the measurement range.

In this study, we present a compact, cost-effective Fizeau fiber-based DMI module. We propose and implement a novel method called the dynamic current-wavelength phase-generated carrier (PGC) technique, which enhances the accuracy and stability of measurements while significantly extending the measurement range. Furthermore, we introduce a laser wavelength stabilization method rooted in hydrogen cyanide (HCN) gas absorption within the 1550 nm wavelength range.

2. DYNAMIC CURRENT-WAVELENGTH PGC METHOD

The theoretical model derivation for the proposed dynamic current-wavelength PGC method is presented below.

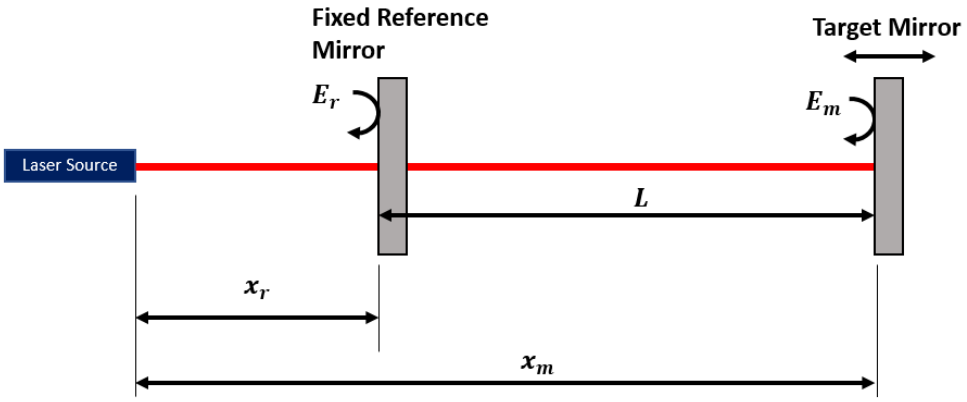

Figure 1 Schematic of the developed Fizeau interferometer.

In the proposed method, the injection current of the laser diode is controlled to achieve wavelength modulation. Eq. (1) expresses the modulated interference signal, in which I is the intensity of the interference signal; A represents the DC term of the signal; B corresponds to the amplitude of the interference signal; L is the distance between the reference mirror and target mirror as shown in Figure 1; ν refers to the optical frequency of the laser, and c signifies the speed of the light, ν_0 denotes the laser's center frequency, $\delta\nu_{\mathrm{PGC}}$ is the optical frequency modulated amplitude; and, ω_{mod} represents the modulation frequency.

$$I = A + I_{mod}\cos(\omega_{mod}t) + B\cos\left(\frac{4\pi L}{\lambda_o} + \frac{4\pi L}{c}\delta\nu_{PCG}\cos(\omega_{mod}t)\right) \quad (1)$$

The injection current is modulated, which in turn results in the modulation of the light's intensity. In Eq. (2), I_{mod} stands for the intensity of the light is modulated and λ_o is the center wavelength of the laser.

$$\begin{aligned} I = A + [I_{mod} - 2J_1(C)]\cos(\omega_{mod}t)\sin(2kL) \\ + B[\cos(2kL)[J_0(C) + 2\sum_{n=1}^{\infty}(-1)^n J_{2n}(C)\cos(2n\omega_{mod}t) \\ + \sin(2kL)[2\sum_{n=2}^{\infty}(-1)^n J_{2n-1}(C)\cos((2n-1)\omega_{mod}t)] \end{aligned} \tag{2}$$

The Jacobi–Anger expansion of Eq. (1) is Eq. (2). J_{i} represents the Bessel function of the first kind, and $\mathrm{k} = 2\pi/\lambda$ is the wave number. Based on Eq. (2), we see that a quadrature signal carrying displacement information, represented by cos(2kL) and sin(2kL), can be modulated onto the odd and even harmonics of the modulation frequency.

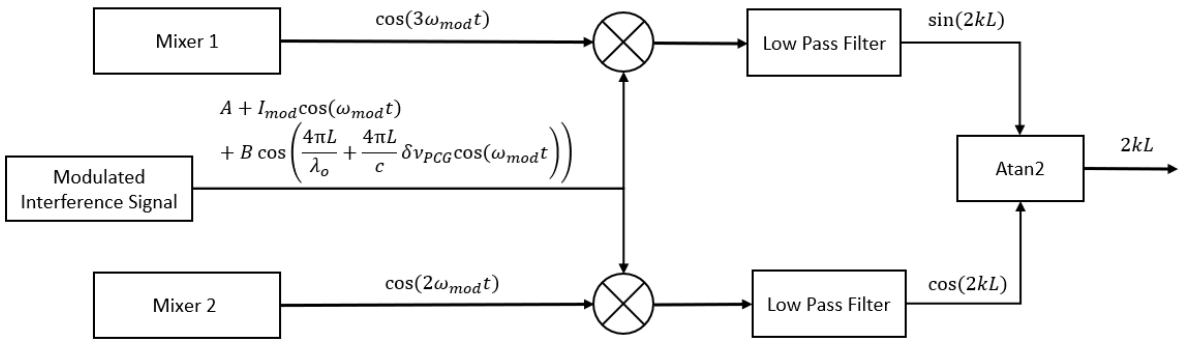

Figure 2 Dynamic current-wavelength PGC demodulation process.

The modulated interference signal first undergoes a mixing process in the demodulation process. This mixed signal is then subject to low-pass filtering, which extracts the quadrature signal. The interference phase, as represented in Eq. (3), is obtained by calculating the arctangent of the quadrature signal. This phase can subsequently be converted into a displacement value. Figure 2 visually illustrates the process of demodulation.

$$\mathrm{Arctan}\left(\frac{J_3(C)\sin(2kL)}{J_2(C)\cos(2kL)}\right) = 2kL \quad \text{when} \quad C = 3.77 \tag{3}$$

Eq. (2) demonstrates that the intensity modulation is incorporated into the first harmonic. Many PGC methods employ the modulated frequency's first and second harmonics as mixers, as outlined in references [10, 15]. However, in the dynamic current-wavelength PGC method, using the first and second harmonics to extract the quadrature signal may introduce an error due to the intensity modulation. Figure 3 presents a simulation of the interference signal and the demodulated phase when the target mirror moves at a constant speed. The results reveal that the demodulated phase suffers from periodic errors, and the center of the Lissajous circle is not situated at the origin. We use the third and second harmonics to circumvent this error to extract the quadrature signal.

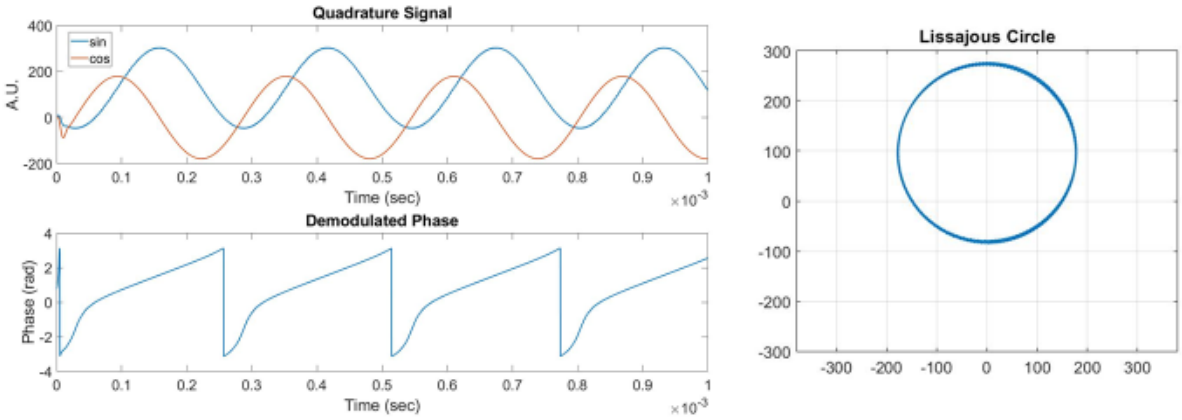

Figure 3 Simulation result of using first and second harmonic as the mixers.

Eq. (3) demonstrates that the computed interference phase is only accurate if the amplitudes of the quadrature signals are identical. In this scenario, the amplitude of the quadrature signal depends on the modulation depth, denoted as C. Specifically, when C equals 3.77, the amplitude of the quadrature signal matches that depicted in Figure 4.

Eq. (4), on the other hand, indicates that in the traditional current-wavelength PGC method, the modulation depth is influenced by the distance, L. This connection restricts the measurement range of the method. If the distance undergoes substantial changes, one of the quadrature signals may dwindle to zero, leading to a failure in phase computation.

$$C = \frac{4\pi L \delta\lambda}{\lambda_0^2} \tag{4}$$

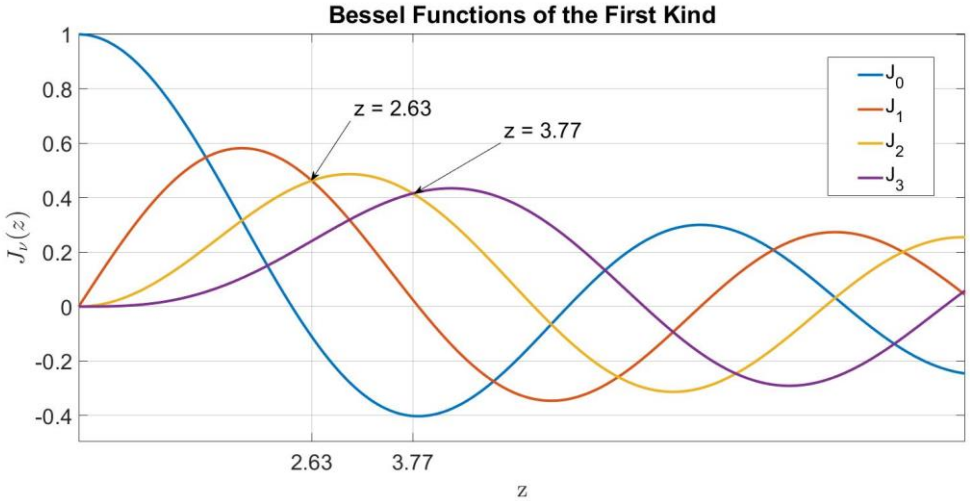

Figure 4 Bessel function of the first kind.

Thus, it is crucial to ascertain the value of distance L to maintain a fixed modulation depth. We suggest the adoption of frequency scanning interferometry (FSI) [16, 17] for the measurement of distance L, enabling the wavelength-modulated amplitude ($\delta\lambda$) to function as a distance variable. When the modulation depth is set at 3.77, we can derive Eq. (5). It's important to note, however, that while the accuracy of these measurements may not match those

of the incremental interferometer, they can be sufficient to determine the amplitude of optical frequency modulation.

$$\delta\lambda = \frac{0.943\lambda_0^2}{L} \tag{5}$$

In traditional interferometry, the wavelength is typically constant while the distance to the target mirror (L) varies. Contrastingly, in frequency scanning interferometry (FSI), the wavelength undergoes a linear scan. Eq. (6) illustrates the optical frequency sweeping in FSI, where $\delta\nu_{FSI}$ denotes the sweeping depth, and T signifies the sweeping period. Suppose the distance to the target mirror (L) remains stable during scanning. In that case, the phase shift of the interference signal becomes proportional to the distance (L), as shown in Eq. (7). By measuring this phase shift of the interference signal, the distance can be inferred as depicted in Eq. (8).

$$\nu_{FSI}(t) = \nu_0 + \frac{\delta\nu_{FSI}}{T}t;\ 0 < t < T \tag{6}$$

$$\Delta\phi = \frac{2\pi\delta\nu_{FSI}}{c}L \tag{7}$$

$$L = \frac{c}{2\pi\delta\nu_{FSI}}\Delta\phi \tag{8}$$

3. HCN GAS CELL WAVELENGTH STABILIZATION

The Displacement Measuring Interferometer (DMI) uses the laser's wavelength as a measurement standard, so the wavelength must remain stable and traceable. To this end, our study suggests using an HCN gas cell for laser stabilization. The HCN gas exhibits multiple absorption spectra within the 1550 nm wavelength range. According to the data provided by NIST [18], the wavelength uncertainty attainable with HCN gas can be as precise as 0.2 picometers.

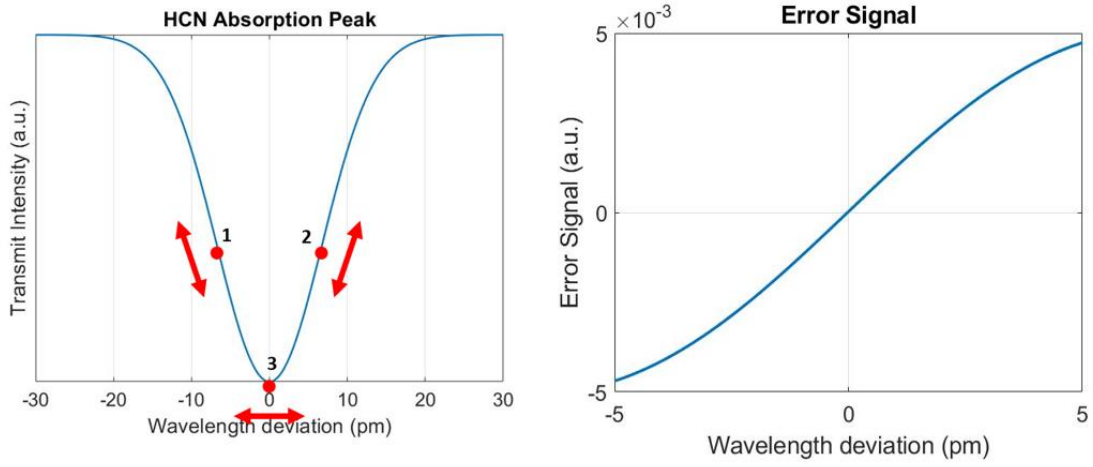

Figure 5 P7 absorption peak of HCN and the wavelength error signal.

In our study, a sinusoidal signal is used to modulate the laser wavelength. Consequently, the Pound-Drever-Hall (PDH) frequency-locking technique can be integrated into our application [19]. This technique blends the transmitted light signal from the gas cell with a signal that maintains the same frequency and phase as the modulation signal. After low-pass filtering, an error signal is produced, representing the wavelength deviation.

Figure 5 (left) illustrates different modulation points on the HCN absorption peak. When the laser's center wavelength is situated at position 1, the modulation and gas cell signals are out of phase, resulting in a negative error signal. Conversely, both signals are in phase when the center wavelength is at position 2, yielding a positive error signal. A zero error signal implies that the central wavelength is at position 3, locked to the absorption line. Figure 5 (right) demonstrates the simulation results depicting the relationship between wavelength deviation and the corresponding wavelength error signal

Given that the wavelength of the diode laser can be modulated by altering the operating temperature, a laser temperature controller, working in tandem with the wavelength error signal and a proportional-integral (PI) controller, can stabilize the wavelength. If the wavelength drifts, the temperature controller modifies the laser's operating temperature based on the error signal. Figure 6 provides a schematic representation of the proposed method for wavelength stabilization.

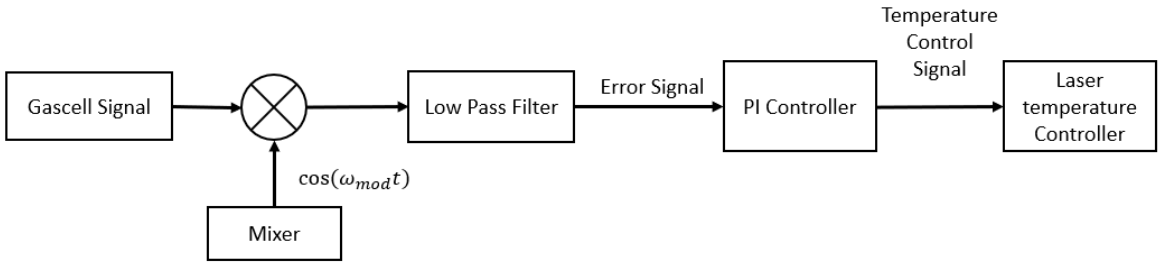

Figure 6 Schematic of proposed wavelength stabilization method [TW Patent].

4. EXPERIMENT SYSTEM CONFIGURATION

Figure 7 illustrates the experimental setup, which can be segmented into several modules: the interferometer module, the interferometer probe module, and the signal and control module. The signal and control module comprises the National Instrument (NI) signal input/output (I/O) chassis, a laser temperature, and a current controller.

The operational principle of the experimental system is as follows: The interferometer probe module captures the interference signal and conveys it to the interferometer module via optical fibers. The interferometer module, in turn, transmutes the optical interference signal into an electrical one and relays it to the NI chassis. The signal can then be read via an industrial personal computer (IPC), and demodulation algorithms can be implemented to convert the interference signal into displacement data.

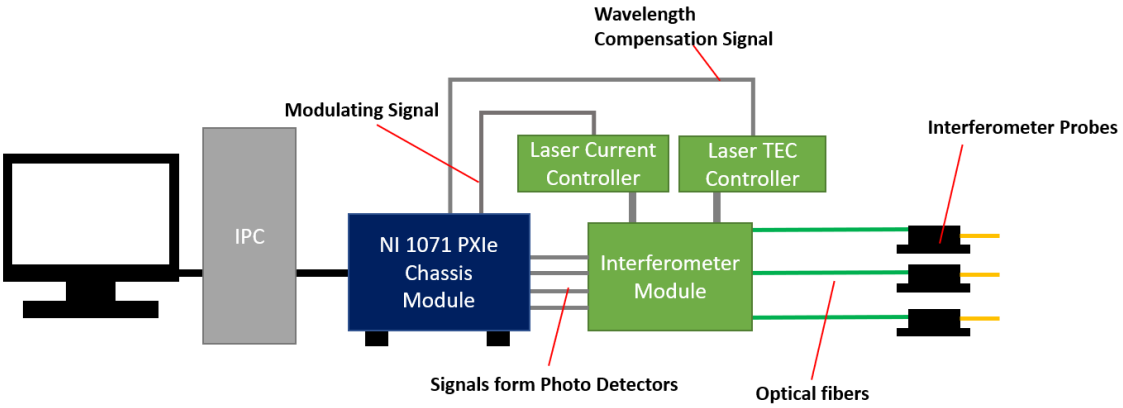

Figure 7 Schematic of the proposed interferometer system [TW Patent].

4.1 Interferometer probe module

This study aims to minimize the influence caused by environmental disturbances. We utilize a Fizeau interferometer configuration that maximizes the common optical path. Figure 8 shows the proposed fiber Fizeau interferometer probe. The reference beam reflects from the end face of the FC/PC fiber connector, and the collimator intentionally uses an FC/APC connector, which has an 8-degree angle. The design prevents multi-beam interference and eliminates the need for additional external beam splitters. Furthermore, this design maintains a common optical path until the FC/PC fiber connector's end face, making the system less susceptible to environmental disturbances.

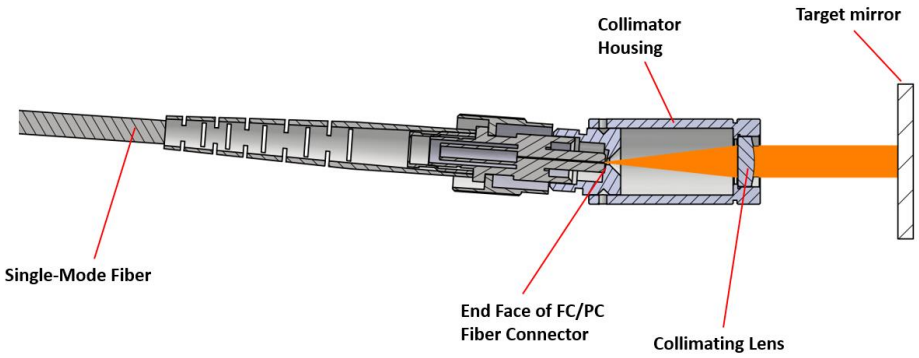

Figure 8 Proposed fiber-coupled Fizeau interferometer probe [TW Patent].

4.2 Interferometer module

Figure 9 presents the schematic of the interferometer module. A 1550 nm fiber-coupled DFB laser diode serves as the light source. The emitted light is divided into two paths by a 90:10 fiber splitter. The bulk of the light (90%) is guided through an attenuator for intensity modulation. Post-attenuation, the light is split by a 1x4 fiber splitter. Three output paths from this splitter are linked to port 1 of individual fiber circulators. Light entering port 1 is redirected to port 2, which is connected to the fiber connector of the interferometer probe. The interference signal detected by the probe is reflected in port 2 and subsequently guided to port 3 by the fiber circulator. Port 3 is connected to the photodetector (PD), responsible for converting the optical

interference signal into an electrical one. This electrical signal is then relayed to the input/output module of the NI system.

The remaining light (10%), split by the initial fiber splitter, traverses through an HCN gas cell. Light that passes through the gas is directly linked to PD4. It is worth noting that all the fiber components in the diagram utilize FC/APC connectors for their fiber connectors to minimize noise induced by reflected light.

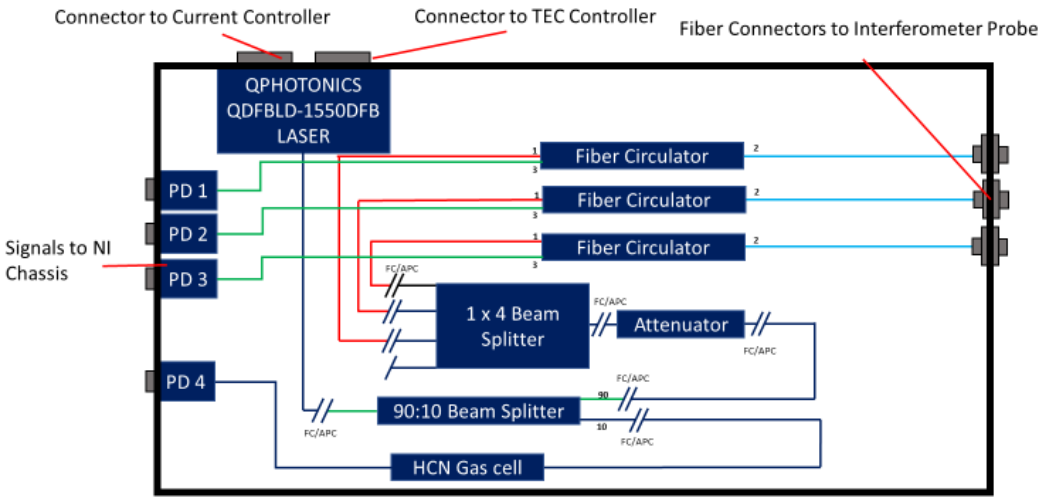

Figure 9 Schematic of interferometer module [TW Patent]

4.3 Algorithm of dynamic current-wavelength PGC method

For the demodulated quadrature signals to have identical amplitudes, the modulation depth must be fixed at 3.77. As such, the system needs to dynamically adjust the amplitude of the wavelength modulation contingent on the reference mirror's position. It should be noted that the central wavelength of the laser is locked at 1547.435 nm, corresponding to the P7 absorption peak of the HCN gas cell.

Figure 10 presents the algorithm associated with the dynamic current-wavelength PGC method. When the system is reset or the interferometer is zeroed, Frequency Scanning Interferometry (FSI) is initially utilized to assess the distance L between the target mirror and the reference mirror. Subsequently, Eq. (5) is employed to compute the wavelength-modulated amplitude. The measured displacement can then be tracked by integrating it with the initially calculated distance, and the amplitude of the wavelength modulation can be controlled to uphold the modulation depth at 3.77 consistently.

5. EXPERIMENT RESULTS

5.1 Stability test

A stability test was conducted by positioning the interferometer probe near a fixed target mirror. Given the concise optical path length difference between the reference mirror and the target mirror, any wavelength or air refractive index variations would have minimal impact on the measured values. Hence, if the acquired data demonstrate considerable drift, it signifies the

system's instability. As shown in Table 1, the proposed system's standard deviation over a 1-minute is 0.7 nm, while the standard deviation over a 10-minute interval is 3.4 nm.

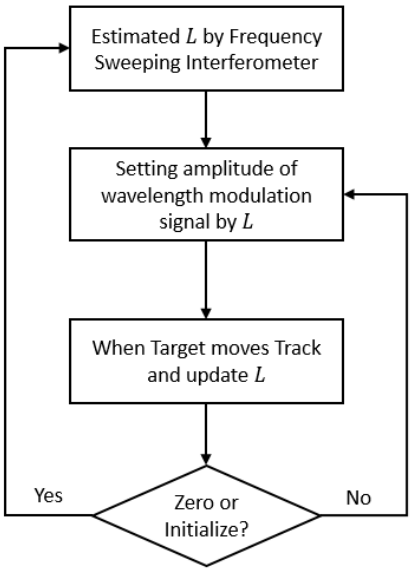

Figure 10 Algorithm of dynamic current-wavelength PGC method [TW Patent].

Table 1 Stability testing results

Period	**Standard deviation (nm)**
1 Minute	0.7
10 Minutes	3.4

Furthermore, the data collected over 10 minutes can discern a drift phenomenon. This situation is likely attributable to changes in temperature, which lead to the expansion or contraction of the fixed mechanism, culminating in alterations in the distance between the reference mirror and the target mirror. These results underscore that the proposed interferometer can measure displacements at nanometer scales or even smaller, provided that environmental factors and wavelength variations are effectively managed.

5.2 Long-range displacement measuring experiment

To verify the effectiveness of the displacement measurement module developed in this research, the interferometer probe was installed on a wafer measurement machine constructed at the Precision Metrology Lab at National Taiwan University. The experimental setup is depicted in Figure 11. The actuating system employs the Aerotech ABL80040 air-bearing stage, capable of a travel range of 300 mm in both X and Y axes.

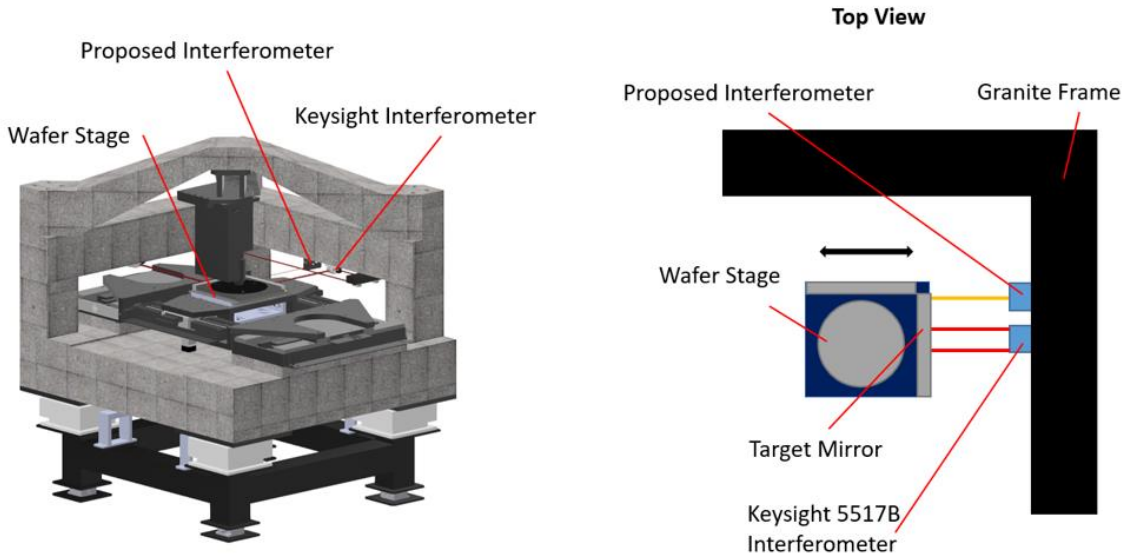

Figure 11 Long-range displacement measuring setup [TW Patent].

In this experiment, the wafer machine moves at 10, 50, 100, 200, and 300 mm displacements, each distance being repeated 90 times. The interferometer probe proposed in this study and the calibrated Keysight 5517B interferometer was installed beneath the machine's granite beam to measure the displacements simultaneously. The experimental results are outlined in Table 2. The discrepancy between the proposed interferometer and the commercial interferometer within a 300 mm displacement is within ±40 nm. This situation suggests a high degree of agreement between the proposed module and the calibrated Keysight system when measuring long-range displacements. Additionally, the standard deviation of the differences is within 35 nm, indicating minimal variations in the measured differences for identical displacements, thus showcasing the system's precision.

Table 2 Result of long-range displacement measuring experiment.

Displacement (mm)	STD of proposed Interferometer module(nm)	STD of Keysight 5517B interferometer (nm)	Average deviation (nm)	STD of Deviation (nm)
10	11.9	13.1	-20.6	15.9
50	15.9	15.4	6.2	17.6
100	22.6	21.1	39.9	22.6
200	25.9	22.3	-35.5	20.4
300	44.3	28.0	10.0	34.4

Furthermore, it's notable that even when the measured displacement reaches 300 mm, the system can still maintain a deviation within tens of nanometers. This result highlights the effective mitigation of the limitations associated with the current carrier wavelength method in measuring long-range travel, as proposed in this study.

6. CONCLUSIONS

This research presents a fiber-optic Fizeau interferometer for displacement measurement, overcoming multiple-beam reflection issues using angled fiber connectors. The novel dynamic current-wavelength PGC method is introduced for carrier modulation, maintaining the consistent amplitude of demodulated quadrature signals across various distances and

outperforming previous wavelength-carrying techniques. Laser frequency stabilization is achieved via an HCN gas absorption method and dynamic temperature adjustment. The developed interferometer showed impressive static stability of 0.7 nm within a minute and consistency with a calibrated laser interferometer, with bias errors within 40 nm over 300 mm. These findings open new avenues for improvements and applications in precision measurement, beneficial for inline semiconductor manufacturing processes.

REFERENCES

[1] R. Kneppers and A. Amstelveen, "HP laser interferometers," *Vaisala news,* vol. 151, pp. 34-37, 1999.

[2] F. Shabahang and S. T. Smith, "Multi-axis modulated compact fiber-based Fabry–Perot interferometric probe," *Applied Optics,* vol. 61, no. 10, pp. 2768-2774, 2022.

[3] K. Thurner, F. P. Quacquarelli, P.-F. Braun, C. Dal Savio, and K. Karrai, "Fiber-based distance sensing interferometry," *Applied optics,* vol. 54, no. 10, pp. 3051-3063, 2015.

[4] S. Pullteap, "Development of a fiber based interferometric sensor for non-contact displacement measurement," in *International conference on Computer, Electrical, and Systems Science, Paris (France)*, 2010: Citeseer, pp. 1475-1479.

[5] Y. Zhang, K.-N. Joo, and F. Guzman, "Fiber-based two-wavelength heterodyne displacement interferometer," in *Photonic Instrumentation Engineering IX*, 2022, vol. 12008: SPIE, pp. 179-184.

[6] B. Zuanetti, T. Wang, and V. Prakash, "A compact fiber optics-based heterodyne combined normal and transverse displacement interferometer," *Review of Scientific Instruments,* vol. 88, no. 3, p. 033108, 2017.

[7] J. Ishikawa, "TPortable national length standards designed and constructed using commercially available parts-An advanced mechanical design for the iodine stabilized He-Ne laser," *Synthesiology English edition,* vol. 2, no. 4, pp. 246-257, 2009.

[8] L. L. Deck, "Frequency stabilized laser system," ed: Google Patents, 2002.

[9] B. Edlén, "The refractive index of air," *Metrologia,* vol. 2, no. 2, p. 71, 1966.

[10] A. Dandridge, A. B. Tveten, and T. G. Giallorenzi, "Homodyne Demodulation Scheme for Fiber Optic Sensors Using Phase Generated Carrier," *IEEE Transactions on Microwave Theory and Techniques,* vol. 30, no. 10, pp. 1635-1641, 1982, doi: 10.1109/TMTT.1982.1131302.

[11] Z. Yu *et al.*, "High stability and low harmonic distortion PGC demodulation technique for interferometric optical fiber sensors," *Optics & Laser Technology,* vol. 109, pp. 8-13, 2019/01/01/ 2019, doi: https://doi.org/10.1016/j.optlastec.2018.07.055.

[12] A. Zhang and S. Zhang, "High stability fiber-optics sensors with an improved PGC demodulation algorithm," *IEEE Sensors Journal,* vol. 16, no. 21, pp. 7681-7684, 2016.

[13] L. Yan *et al.*, "Precision PGC demodulation for homodyne interferometer modulated with a combined sinusoidal and triangular signal," *Opt. Express,* vol. 26, no. 4, pp. 4818-4831, 2018/02/19 2018, doi: 10.1364/OE.26.004818.

[14] S. Qingping *et al.*, "Performance improvement of phase-generated carrier method by eliminating laser-intensity modulation for optical seismometer," *Optical Engineering,* vol. 49, no. 2, p. 024402, 2/1 2010, doi: 10.1117/1.3294878.

[15] A. V. Volkov, M. Y. Plotnikov, M. V. Mekhrengin, G. P. Miroshnichenko, and A. S. Aleynik, "Phase Modulation Depth Evaluation and Correction Technique for the PGC Demodulation Scheme in Fiber-Optic Interferometric Sensors," *IEEE Sensors Journal,* vol. 17, no. 13, pp. 4143-4150, 2017, doi: 10.1109/JSEN.2017.2704287.

[16] S. Kakuma and Y. Katase, "Frequency scanning interferometry immune to length drift using a pair of vertical-cavity surface-emitting laser diodes," *Optical Review,* vol. 19, pp. 376-380, 2012.
[17] S. Sharma, P. Eiswirt, and J. Petter, "Electro optic sensor for high precision absolute distance measurement using multiwavelength interferometry," *Opt. Express,* vol. 26, no. 3, pp. 3443-3451, 2018/02/05 2018, doi: 10.1364/OE.26.003443.
[18] S. L. Gilbert, W. C. Swann, and C.-M. Wang, "Hydrogen cyanide H13C14N absorption reference for 1530 nm to 1565 nm wavelength calibration–SRM 2519a," *NIST special publication,* vol. 260, p. 137, 2005.
[19] E. D. Black, "An introduction to Pound–Drever–Hall laser frequency stabilization," *American journal of physics,* vol. 69, no. 1, pp. 79-87, 2001.

CONTACTS

Prof. Dr.-Ing. Liang-Chia Chen email: lchen@ntu.edu.tw

